Kinetic and Thermodynamic Study of Methylene Blue Adsorption onto Chitosan: Insights about Metachromasy Occurrence on Wastewater Remediation

Julian S. Kellner-Rogers[a], Jeffrey Taylor[a], Arvid M. Masud[b], Nirupam Aich[b], Alexandre H. Pinto[a]*

[a]Ithaca College, Department of Chemistry, Center for Natural Sciences, 953 Danby Road, Ithaca, NY, 14850

[b]University at Buffalo, The State University of New York, Department of Civil, Structural and Environmental Engineering, 232 Jarvis Hall, Buffalo, NY, 14260

*Corresponding Author: Email: apinto2@ithaca.edu, Phone: (607) 274-7752, Fax: (607) 274-1848

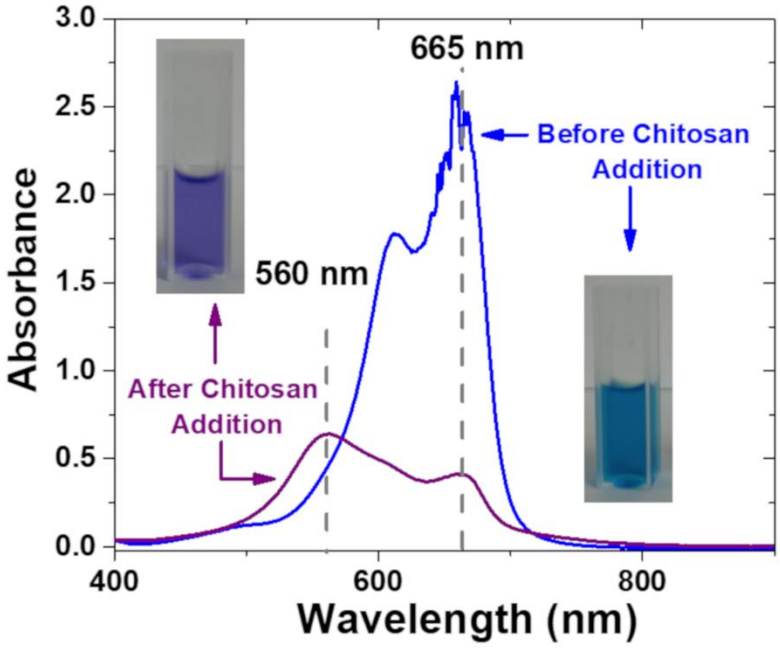

Graphical Abstract: Absorption spectra of methylene blue before and after contact with chitosan, showing that the absorption spectrum and color of methylene blue changes due to metachromasy induced by chitosan.

Abstract

Methylene Blue (MB) is a dye frequently used in the textile industry and a potential wastewater pollutant. MB adsorption onto the surface of solid materials is a promising method for wastewater remediation. The biopolymer chitosan is one of the promising candidates as an adsorbent for MB removal from wastewater. However, the contact between MB and chitosan induces the aggregation of MB molecules. The formation of MB aggregates can lead to an appearance of additional bands in the MB visible absorption spectrum. This phenomenon is called metachromasy. In this paper, chitosan was used as adsorbent to study the kinetics and thermodynamic parameters related to the elimination of MB as single molecules (Sng-MB) and aggregates (Agg-MB) species from simulated wastewater. It was found that, for MB single molecules or aggregates, the adsorption process follows the pseudo second order adsorption kinetics model. For each temperature studied, Agg-MB always presented higher rate constant than Sng-MB, indicating a faster adsorption of Agg-MB in comparison to Sng-MB. Additionally, the adsorption process presented a lower activation energy for Agg-MB, indicating Agg-MB adsorption is favored in relation to Sng-MB. The thermodynamic studies indicated the adsorption process for both MB species is endothermic and spontaneous from 298 to 348 K. The adsorption isotherms could be properly fitted and interpreted according to Temkin and Dubinin-Radushkevich models. Studies varying the initial pH of MB solution indicated that metachromasy could be suppressed in acidic pH values, whereas alkaline pH values led to an increase in the removal percentage of Sng-MB and Agg-MB in relation to neutral conditions. The analysis of chitosan powder before and after adsorption indicated the adsorption process does not cause structural changes to the chitosan. The kinetic and thermodynamic study of the relative adsorption of MB single molecules and aggregates onto chitosan can provide fundamental information for MB wastewater remediation.

Keywords

Methylene Blue / Chitosan / Metachromasy / Wastewater Remediation / Adsorption

1. Introduction

Water contamination is a serious environmental issue that requires specific fundamental questions to be addressed. One of the main contaminants found in the aquatic environment are synthetic dyes; it is estimated that over 1.6 million tons of dyes are produced annually worldwide[1,2]. Although there is no accurate data about how much of this dye production is discharged in the environment, it is estimated that around 2% is discharged as production waste, and 1-10% is discharged as a consumption waste[3].

Methylene blue (MB) is a cationic phenothiazine dye used in a variety of industrial applications, such as textile and hair dyeing and biological tissue staining[4,5]. Despite its low toxicity, acute exposure to MB has been described to cause side effects, like cyanosis, nausea, vomiting, and increased heart rate[6]. Additionally, MB can be harmful to aquatic life, since its presence in water can severely reduce sunlight penetration, affecting nutrient production by autotrophic aquatic organisms[7,8].

The absorption spectrum of MB in the visible range of the electromagnetic spectrum presents a main band centered on 665 nm, which is related to single molecules of MB and gives a blue coloration to MB aqueous solutions. However, it has been described in the literature that, upon contact with certain materials, MB aqueous solutions change their color from blue to a purple hue[9–12]. This color change phenomenon is called metachromasy (also called metachromasia)[13,14], and in the case of MB, the color change is accompanied by the appearance of a new absorption band at lower wavelength, around 560 nm, which can be explained by the formation of MB aggregates higher than MB dimers. This new band appears at lower wavelength because of the electrostatic repulsion between the π electron systems of MB cations upon

aggregation[15]. Among the materials recognized for inducing MB metachromasy are: clays[16], graphene oxide[17], and silica (SiO_2) coated magnetite (Fe_3O_4) nanoparticles[18].

Adsorption of the dyes onto safe and harmless adsorbents has proven to be a clean and effective method to remove the dyes from wastewater[19]. A promising adsorbent is chitosan, which is derived from chitin, the second most abundant natural polymer after cellulose and found in crustacean shells, such as crabs and prawns[20]. The abundance of chitin and its straightforward deacetylation conversion process to chitosan make chitosan a cost-effective material for several applications, such as drug delivery, cosmetic products, tissue engineering, and food processing[21]. Furthermore, the low solubility of chitosan in water facilitates its easy separation from water after the decontamination process[22].

Chitosan in different forms, for instance, powders and beads and composite materials containing chitosan, are recognized to induce metachromasy in MB. For instance, Csoka and co-workers observed metachromasy while staining chitosan with MB by looking at chitosan under a visible light microscope in linearly polarized light[23]. Hirano and co-workers observed metachromasy in MB when interacting with sulfate derivatives of chitosan[24].

Despite the recognized occurrence of MB metachromasy due to interaction with chitosan, there are no studies describing how different MB species, when simultaneously present, behave in relation to adsorption onto chitosan surface. Thus, in this paper, chitosan was used as an adsorbent for removal of MB from simulated wastewater to verify how the presence of single MB molecules and MB aggregates (hereafter referred, respectively, by the acronyms Sng-MB and Agg-MB) affects the adsorption process at different temperatures and pH values. The results were used to describe the kinetic and thermodynamic parameters governing the adsorption process, in addition to determining the isotherm model that best describes the process.

2. Materials and Methods

2.1 Materials

Chitosan (85% deacetylated, Alfa Aesar, 15 kDa), chitin (Alfa Aesar, 15 kDa), methylene blue hydrochloride (Acros Organic), hydrochloric acid (HCl, Mallinckrodt Chemicals, 36.5-38%), and sodium hydroxide (NaOH, VWR) were used without further purification.

2.2 Characterization Techniques

The UV-vis absorption spectra were collected in an Agilent 8453 spectrophotometer with wavelength ranging from 190 to 1100 nm. The infrared (IR) spectra were collected in a Thermo Scientific Nicollet 6700 FT-IR spectrometer in the transmittance mode with wavenumber between 600 and 4000 cm^{-1} from samples prepared by mixing the material with potassium bromide (KBr) and forming compact transparent pellets using a hydraulic press. The powder X-ray diffraction (XRD) patterns were collected in a Shimadzu Lab-X XRD 6000 equipped with CuKα radiation (0.15406 nm), operating at 30 kV and 30 mA, with 2 θ ranging from 5 to 65 °, with a step size of 0.0200 °, totaling a time around 2 h of collection per sample. The diffuse reflectance spectra at visible range was collected in solid samples mixed with barium sulfate in a Shimadzu UV-2101 PC equipped with integrating sphere.

The zeta potential values of the MB samples before and after adsorption were determined by measuring the electrophoretic mobility (EPM) of the samples in aqueous phase using a Malvern ZetaSizer Nano ZS (Malvern Instruments Ltd., Westborough, MA). Moreover, dynamic light scattering (DLS) was performed using the ZetaSizer to determine the hydrodynamic diameters,

i.e., aggregate sizes of MB before and after the adsorption onto chitosan. The MB aqueous samples were diluted to 50 times their suspension concentration with DI water prior to zeta potential and DLS studies.

Specific surface areas of the chitosan samples before and after MB adsorption were determined from N_2 adsorption isotherm obtained at − 196 °C (Tri-Star II 3020, Micromeritics Instrument Corp., Norcross, GA). Chitosan samples were first degassed at 120 °C for 3 h before analysis. The Brunauer–Emmett–Teller (BET) equation was applied to N_2 adsorption data for P/P_0 between 0.01 and 0.1.

For scanning electron microscopy (SEM), the chitosan samples were dispersed in methanol, sonicated for 30 minutes, deposited onto silicon substrates, and the substrate edges were painted with carbon conductive ink to avoid sample charging during imaging due to the insulating character of chitosan. The scanning electron microscope was a Field Emission Gun (FEG) Tescan Mira 3, operating at 10 kV.

2.3 Batch adsorption studies

A methylene blue hydrochloride stock solution of 8.0×10^{-4} mol/L (300 mg/L) was prepared by dissolving g of methylene blue hydrochloride in 200 mL of double distilled water. This stock solution was diluted multiple times to produce a calibration curve for concentrations ranging from 6.7×10^{-6} mol/L (2.5 mg/L) to 5.3×10^{-5} mol/L (20 mg/L).

For batch adsorption experiments, the 8.0×10^{-4} mol/L stock solution was diluted to produce 30 mL of a 4.0×10^{-5} mol/L (15 mg/L) MB solution. The solution was taken to the desired temperature, using either an oil bath, for 298, 323, and 343 K, or an ice bath, for 273 K.

An UV-vis absorption spectrum was collected from this solution, revealing a highest intensity peak centered at 665 nm, which is related with the Sng-MB. Then, 0.5 g of chitosan was added to the MB solution upon continuous stirring at 500 rpm provided by an overhead stirrer, and 30 seconds after the chitosan addition, another aliquot was collected, and its UV-vis absorption spectrum was recorded, revealing the appearance of a peak at 560 nm, which is related to Agg-MB, in addition to the peak previously observed at 665 nm. Tto study the peaks for Sng-MB and Agg-MB, this aliquot collected 30 seconds after chitosan addition was considered the point 0 minutes on the kinetics studies. The aliquot collection proceeded every 6 minutes until completion of 60 minutes after chitosan addition.

For each collected aliquot, the solid was separated from the liquid part by centrifuging at 3000 rpm for 5 minutes, and the respective UV-vis spectra of the liquid part were collected. The intensity of the peaks at 560 and 665 nm were monitored. For the peak at 665 nm, the intensity was converted to molar concentration by using the equation obtained from the calibration curve to determine the molar concentration of Sng-MB. For the peak at 560 nm, the intensity was converted to molar concentration by using the extinction coefficient value as calculated by Rabinovich and Epstein[25] to determine the molar concentration of Agg-MB.

The percentage of removal for MB single molecules and aggregates from the solution was calculated according to equation (1):

$$Removal\ Percentage\ (\%) = \left(1 - \frac{C_t}{C_0}\right) \times 100\% \quad \text{.....(1)}$$

The adsorption capacity (q_t) of the MB single molecules and aggregates onto chitosan versus time was calculated using equation (2):

$$q_t = \frac{(C_0 - C_t)}{m} \times V \text{.....(2)}$$

Where C_0 is the Sng-MB or Agg-MB initial concentration in mol/L, C_t is the concentration remaining in solution in a certain time point in mol/L, V is the total volume of solution (30 mL), and m is the mass of chitosan (0.5 g). Consequently, q_t is measured in (mol of MB/g of chitosan). The batch adsorption experiments were performed in duplicates, and the results presented are the average of the two trials.

All the concentrations were used in mol/L instead of mg/L to facilitate the comparison between the Sng-MB and Agg-MB in terms of number of moles, since the exact molecular weight of Agg-MB species is not known.

2.3.1 Kinetic Study:

The adsorption capacity versus time (q_t) data was used to study the kinetic model underlying the adsorption process for both Sng-MB and Agg-MB. Four models were tested: Pseudo first order, pseudo second order, intraparticle diffusion, and Elovich models.

For the pseudo first order model, the linear equation used to analyze the data was equation (3):

$$\log(q_e - q_t) = \log(q_e) - \frac{k_1}{2.303} t \text{.....(3)}$$

Where q_e is the adsorption capacity at equilibrium (mol/g), and k_1 is the rate constant for a pseudo first order process (min^{-1}). q_e and k_1 were calculated, respectively, from the intercept and the slope of a log (q_e-q_t) vs time graph[26].

The pseudo second order model was represented by equation (4):

$$\frac{t}{q_t} = \frac{1}{k_2 \times q_e^2} + \frac{1}{q_e} t \text{.....(4)}$$

Where k_2 represents the rate constant (measured in $g.mol^{-1}.min^{-1}$) for the pseudo second order model, which could be calculated from the intercept of t/q_t vs time graph[26,27].

The intraparticle diffusion model was calculated according to equation (5):

$$q_t = k_{id} t^{0.5} + C \text{.....(5)}$$

Where k_{id} ($mol.g^{-1}.min^{-0.5}$) is the intraparticle diffusion rate constant that can be calculated from the slope of qt vs $t^{0.5}$ graph, and C is the graph intercept[26,28].

The Elovich model was calculated according to equation (6):

$$q_t = \beta \ln(\alpha\beta) + \beta \ln(t) \text{.....(6)}$$

Where α is the initial adsorption rate ($mol.g^{-1}.min^{-1}$), and β is the desorption rate ($mol.g^{-1}$)[26,28].

2.3.2 Activation Energy Calculation:

After concluding the best kinetic model for the adsorption process, the activation energy was calculated by inserting the rate constant values of the most suitable model into the Arrhenius equation:

$$ln\frac{k_A}{k_B} = -\frac{E_a}{R}\left(\frac{1}{T_A} - \frac{1}{T_B}\right) \text{.....(7)}$$

Where E_a is the activation energy (J/mol), R is the gas constant (8.314 J/mol.K), k_A and k_B are the rate constants, respectively, at temperatures A and B[29].

2.3.3 Thermodynamic Parameters Calculation:

The ΔH and ΔS for the adsorption process of Sng-MB or Agg-MB were estimated by plotting a graph of ln K vs 1/T, which describes the van't Hoff equation (eq. (8)).The ΔH and ΔS were determined, respectively, from the slope and intercept of the van't Hoff plot[30]:

$$lnK = \frac{\Delta S}{R} - \frac{\Delta H}{RT} \text{.....(8)}$$

Where K is the equilibrium constant for the adsorption process, which was calculated according to equations (9 a) or (9 b)[31,32]:

$$K = \frac{C_{adsorbed}}{C_e} \text{.....(9 a)}$$

$$K = \frac{q_e \times m}{C_e \times V} \text{.....(9 b)}$$

Where $C_{adsorbed}$ and C_e are the MB species molar concentration, respectively, adsorbed onto chitosan and remaining in solution at equilibrium obtained from the batch adsorption experiments; q_e is the adsorption capacity at equilibrium obtained from the batch adsorption experiments; m is the mass of chitosan used in the experiment (0.5 g), and V is the volume of MB solution (30 mL).

The derivation confirming the equivalence between equations (9 a) and (9 b) is shown in the Supporting Information.

The ΔG of the adsorption process of MB species onto chitosan was determined according to equation (10):

$$\Delta G = \Delta H - T\Delta S \text{.....(10)}$$

2.3.4 Adsorption Isotherms Study:

For the isotherm studies, the methylene blue hydrochloride stock solution of 8.0 x 10^{-4} mol/L (300 mg/L) was diluted for three different concentrations in the range between 2.7 x 10^{-5} mol/L (10 mg/L) and 8.0 x 10^{-5} mol/L (30 mg/L) and set to the desired temperature. Then, 0.5 g of chitosan were added to the MB solution upon continuous stirring at 500 rpm provided by an overhead stirrer, and 30 seconds after the chitosan addition, another aliquot was collected, and its UV-vis absorption spectrum was recorded. This aliquot was considered the point 0 minutes for both Sng-MB and Agg-MB. The chitosan-MB system was left to stir, and after 60 minutes, another aliquot was collected, and its UV-vis absorption spectrum was used to calculate the molar concentration and the adsorption capacity of Sng-MB and Agg-MB at equilibrium.

Four different types of isotherms models were studied: Langmuir, Freundlich, Temkin, and Dubinin-Radushkevich (D-R).

Langmuir isotherm implies a monolayer adsorption of the adsorbate onto the adsorbent surface and considers that there is no interaction between two neighboring adsorbate species. The linear form of Langmuir isotherm can be represented by equation (11)[33,34]:

$$\frac{1}{q_e} = \frac{1}{q_m} + \frac{1}{K_L q_m C_e} \text{.....(11)}$$

Where C_e and q_e are, respectively, the molar concentration and adsorption capacity at equilibrium, q_m is the maximum adsorption capacity considering a monolayer (mol/g), and K_L is the Langmuir isotherm constant (L/mol), which is a measurement of the affinity between the adsorbate and the adsorbent. The K_L and q_m parameters can be calculated from a $1/q_e$ vs $1/C_e$ graph.

The Freundlich isotherm implies a multilayer adsorption and heterogeneous distribution of the binding sites onto an adsorbent surface. The linear form of the Freundlich isotherm is given by equation (12)[33,34]:

$$\log q_e = \log(K_F) + \frac{1}{n} \log C_e \text{.....(12)}$$

Where K_F is the Freundlich isotherm constant [(mol/g)(L/g)^n], and n is a dimensionless constant related to the adsorption intensity. K_F and n can be calculated, respectively, from the intercept and slope of a log q_e vs log C_e graph.

The Temkin isotherm implies the heat of adsorption of all adsorbate molecules in the layer would decrease linearly with coverage rather than logarithmically. The linear form of Temkin isotherm is given by equation (13)[33]:

$$q_e = \left(\frac{RT}{K_T}\right)\ln(A_T) + \left(\frac{RT}{K_T}\right)\ln(C_e) \text{.....(13)}$$

Where R is the gas constant (8.314 J/molK), T is the temperature (in K), K_T is the Temkin isotherm constant, and A_T is the Temkin isotherm equilibrium binding constant, measured in (L/mol), which takes into account the adsorbent-adsorbate interactions. K_T and A_T can be estimated from the slope and intercept of a q_e vs ln C_e graph.

The Dubinin-Radushkevich (D-R) is an isotherm based on adsorption potential theory, instead of an assumption of constant adsorption potential or homogeneous coverage of the surface. The linear equation that represents D-R isotherm is given by equation (14)[33,34]:

$$\ln(q_e) = \ln(q_s) - K_{DR}\varepsilon^2 \text{.....(14)}$$

Where q_s is the isotherm saturation capacity (mol/g), K_{DR} is the D-R isotherm constant (mol^2/kJ^2), and ε is the Polanyi potential, which can be calculated according to equation (15):

$$\varepsilon = RTln\left(1 + \frac{1}{C_e}\right) \text{.....(15)}$$

The isotherm constant K_{DR} can be calculated from the slope of a graph of ln q_e vs ε^2, and it is related to adsorption free energy (E) by equation (16):

$$E = \frac{-1}{\sqrt{2K_{DR}}} \text{.....(16)}$$

E is measured in kJ/mol.

3. Results and Discussion

3.1 Batch Adsorption and Kinetics

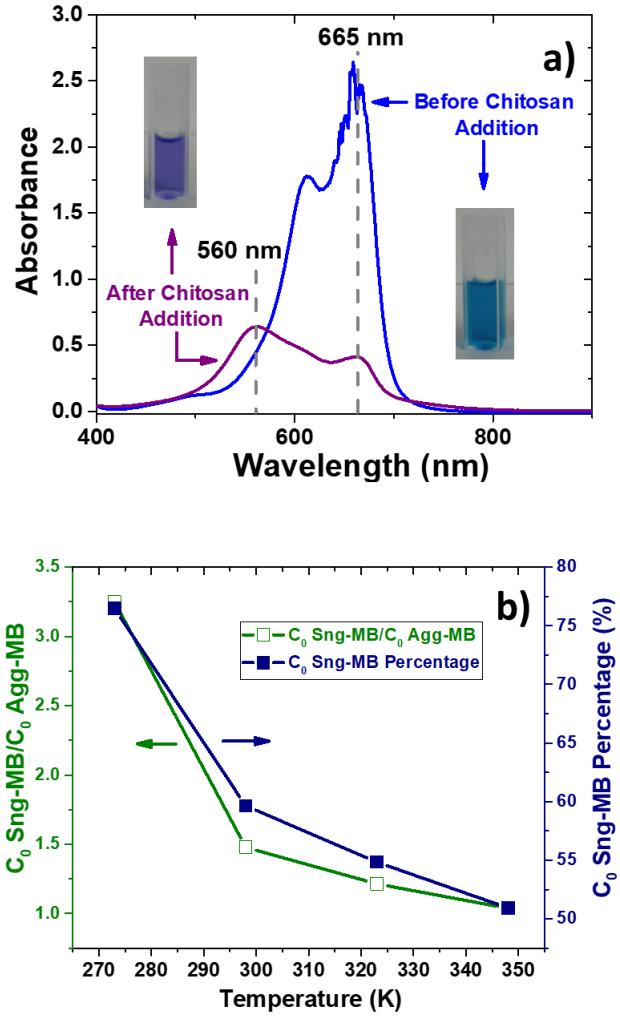

FIG. 1 (a) UV-vis absorption spectra of MB before (blue graph) and after (purple graph) addition of chitosan with pictures of the samples cuvettes in the insets. (b) Variation of the ratio between molar concentration of Sng-MB and Agg-MB (green graph, left axis) and the molar concentration of Sng-MB percentage versus temperature (navy graph, right axis).

Figure 1(a) shows the UV-vis absorption spectra of MB before and after chitosan addition. Before chitosan addition, the spectrum shows one band centered at 665 nm, which is attributed to Sng-MB form[35]. Additionally, the picture of the cuvette containing the sample shows it was a blue liquid. Immediately after chitosan addition, the sample color turned purple, and its absorption spectrum reveals the presence of an additional band at 560 nm, which is attributed to Agg-MB. The coexistence of these two different absorption bands, which is attributed to the presence of MB molecules in different aggregation states, confirm the occurrence of metachromasy.

Figure 1(b) shows how the ratio between the initial molar concentration of Sng-MB and Agg-MB varies with temperature on the left axis and how the percentage of initial molar concentration of Sng-MB in relation to the total initial concentration varies with temperature on the right axis. Both quantities shown vary with the temperature following the same trend. As temperature of the adsorption process increased, the initial molar concentration of Sng-MB decreases, accompanied by an increase in the initial molar concentration of Agg-MB. When the adsorption process was performed at 273 K, the MB solution presented around 75% of Sng-MB right after the addition of chitosan, whereas when the adsorption process was performed at 348 K, the initial concentration of Sng-MB right after chitosan addition decreased to 50%. These results reveal that temperature influences the amount of Agg-MB produced upon contact with chitosan.

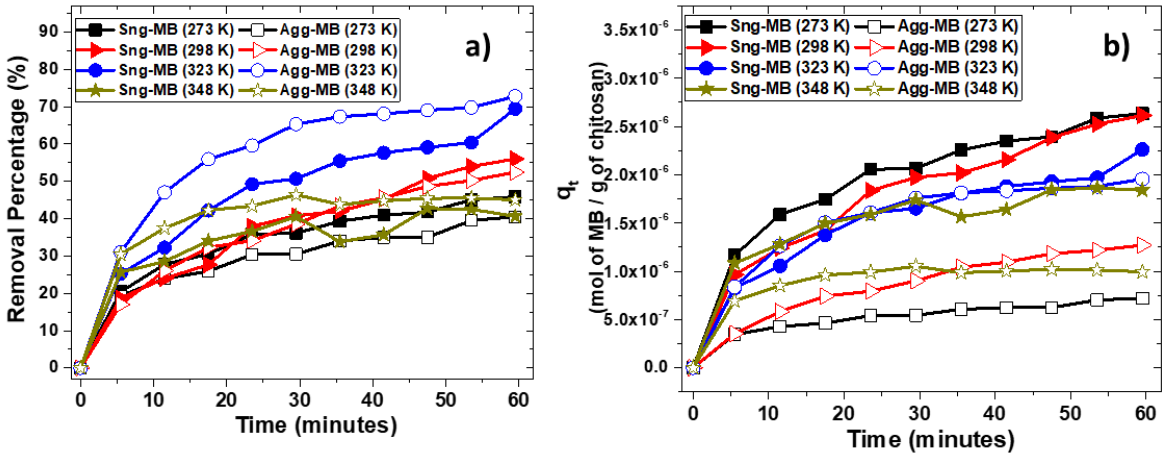

Fig. 2 a) Removal Percentage of Sng-MB and Agg-MB at different temperatures of adsorption experiment versus contact time, b) Adsorption capacity of Sng-MB and Agg-MB at different temperatures of adsorption experiment versus contact time.

Fig. 2 a) shows the removal percentages of Sng-MB and Agg-MB at different temperatures versus contact time during adsorption experiment. In general, the removal percentages of the Sng-MB and Agg-MB species were very close, ranging between 35 and 45 %. The exceptions were the experiments performed at 323 K, where the removal was around 55 and 65 %, respectively, for Sng-MB and Agg-MB. These results indicate 323 K could be an optimum temperature of MB removal by adsorption onto chitosan surface. To prove that no MB removal happened due to dye decomposition at higher temperatures, the MB concentration over time in the absence of chitosan was measured at 323 K, revealing the MB concentration remained constant unless chitosan was present, as shown in Fig. S1 in Supporting Information.

Fig 2 b) shows the adsorption capacity of chitosan for Sng-MB and Agg-MB at different temperatures of adsorption experiment versus contact time. It is observed that the adsorption capacity values for Sng-MB were higher than the ones for Agg-MB at 273 and 298 K. This was

expected since, for these two temperature values, the initial molar concentrations of Sng-MB were higher than the ones for Agg-MB, as shown in Fig. 1 b). For 323 K, where the initial molar concentration of Sng-MB was around 55% of the total initial concentration (Fig. 1 b), the adsorption capacity of chitosan for Sng-MB and Agg-MB was very similar, which can also be related with the fact that 323 K is an optimum temperature for the adsorption experiment. Then, at 348 K, where the adsorbate is formed by approximately 50% Sng-MB and 50% Agg-MB, the chitosan clearly presented a better adsorption capacity for Sng-MB (around 1.8×10^{-6} mol/g) than Agg-MB (around 7.5×10^{-7} mol/g).

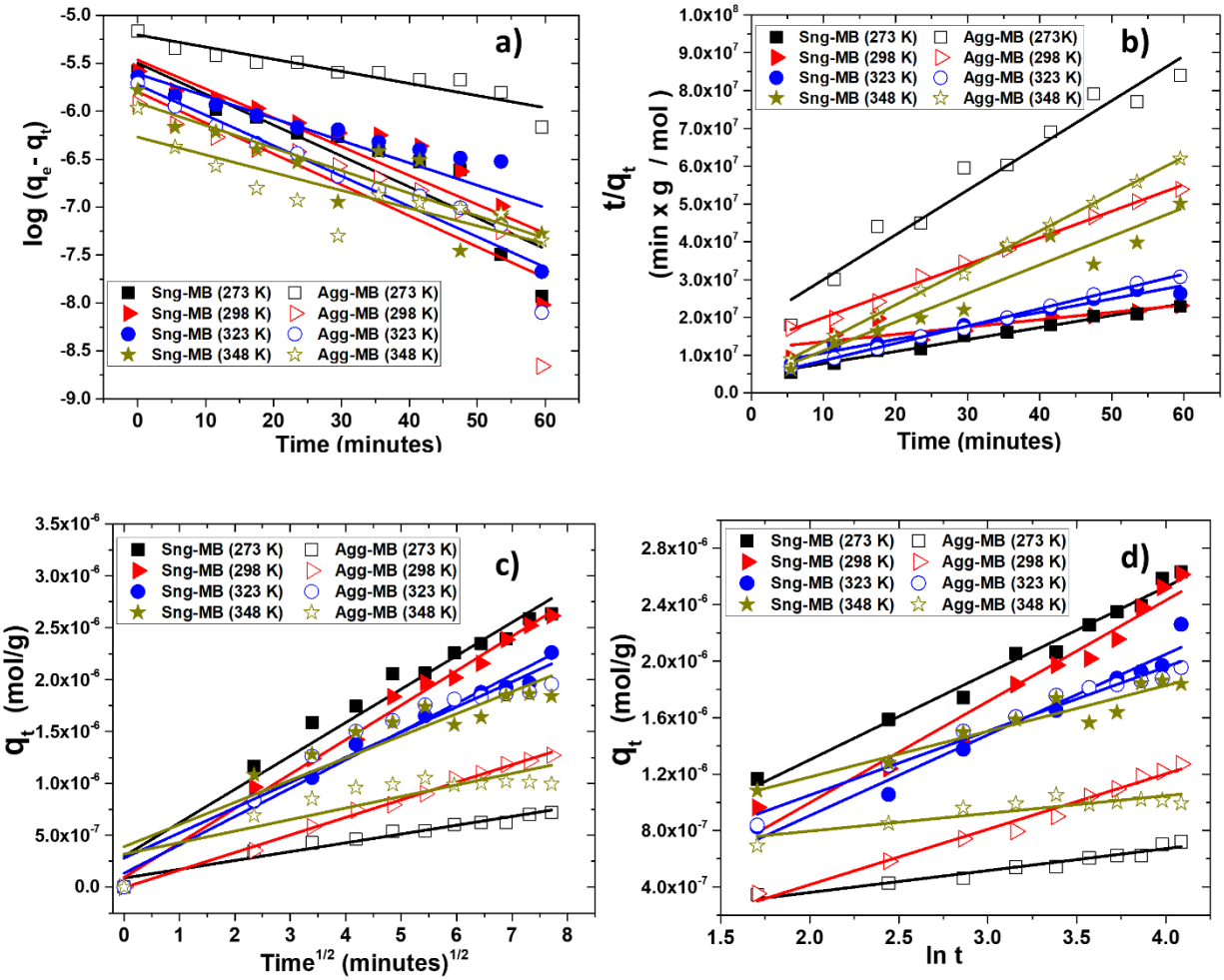

Fig. 3 Linear fitting of the kinetic adsorption models for Sng-MB and Agg-MB at different temperatures of adsorption experiment: a) pseudo first order model, b) pseudo second order model, c) intraparticle diffusion model, and d) Elovich model.

Fig. 3 shows the linear fitting for the kinetic adsorption models for pseudo first order, pseudo second order, intraparticle diffusion, and Elovich models. Visually, it seems that pseudo second order, intraparticle diffusion, and Elovich models presented a good fit to most of the data analyzed. To decide which model fits the data best, the coefficient of determination (r^2) for the linear fitting of each sample was taken in account as presented in Table S1 in Supporting Information.

Table S1 shows the pseudo second order model presents r^2 values closer to 1 for most of the samples, from which it can be concluded that it is the model that best describes the adsorption kinetics of the Sng-MB and Agg-MB onto chitosan in the temperature range studied. From that conclusion, the equilibrium adsorption capacity (q_e) and the pseudo second order adsorption rate constant (k_2) were calculated for Sng-MB and Agg-MB for each temperature as shown in Table 1:

Table 1: Adsorption capacity at equilibrium and rate constant estimated from the pseudo 2nd order adsorption kinetic model.

Sample	q_e (mol/g)	k_2 ($g.mol^{-1}.min^{-1}$)
Sng-MB (273 K)	3.1×10^{-6}	2.6×10^{4}
Agg-MB (273 K)	8.1×10^{-7}	1.1×10^{5}
Sng-MB (298 K)	4.4×10^{-6}	5.2×10^{3}
Agg-MB (298 K)	1.3×10^{-6}	5.1×10^{4}
Sng-MB (323 K)	3.2×10^{-6}	1.2×10^{4}
Agg-MB (323 K)	2.2×10^{-6}	5.1×10^{4}
Sng-MB (348 K)	1.3×10^{-6}	2.2×10^{5}
Agg-MB (348 K)	1.0×10^{-6}	2.6×10^{5}

For each temperature studied, the Sng-MB samples presented higher q_e than the Agg-MB, whereas k_2 is always higher for the Agg-MB than for Sng-MB. The fact that Sng-MB samples have higher q_e than Agg-MB can be explained by the fact that the initial molar concentration of Sng-MB samples is usually higher than the ones for Agg-MB as shown in Fig. 1 b). An indicator of this fact is that the Sng-MB and Agg-MB samples at 348 K present very similar qe, as their initial molar concentrations are practically the same according to Fig. 1 b). Both the Sng-MB and Agg-MB presented an Arrhenius behavior for the relationship of the rate constant with temperature

from 298 to 323 K. By inputting the k_2 values corresponding to 298 and 323 K into equation (7), it was possible to estimate the activation energy (E_a) values for the adsorption process of Sng-MB and Agg-MB onto chitosan, which were equal to 65 kJ/mol and 28 kJ/mol, respectively, for Sng-MB and Agg-MB. The lower activation energy for Agg-MB may indicate a higher probability of adsorption for Agg-MB than for Sng-MB onto chitosan.

3.2 Thermodynamic Results

The van't Hoff plot was graphed according to equation (8), as shown in Fig. 4; the ΔH and ΔS could be, respectively, estimated from the slope and intercept of the van't Hoff plot for both Sng-MB and Agg-MB. Then, these values were plugged into equation (10) to obtain the ΔG values for Sng-MB and Agg-MB in each temperature studied.

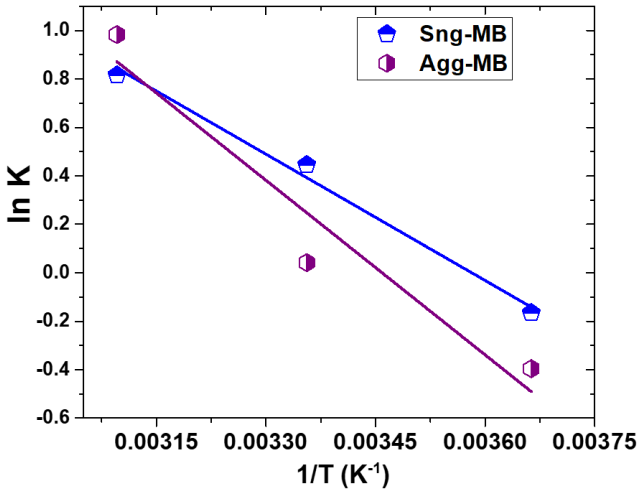

Fig. 4 van't Hoff plot for Sng-MB and Agg-MB species.

Table 2: Thermodynamic parameters ΔH, ΔS, and ΔG for Sng-MB and Agg-MB at different temperatures:

Sample	ΔH (kJ/mol)	ΔS (kJ/mol K)	T(K)	ΔG (kJ/mol)
Sng-MB	14.4	5.17×10^{-2}	273	3.21×10^{-1}
			298	-9.73×10^{-1}
			323	-2.27
			348	-3.56
Sample	ΔH (kJ/mol)	ΔS (kJ/mol K)	T(K)	ΔG (kJ/mol)
Agg-MB	20.0	6.91×10^{-2}	273	1.11
			298	-6.14×10^{-1}
			323	-2.34
			348	-4.07

All the ΔH, ΔS, and ΔG values for Sng-MB and Agg-MB have been listed in Table 2. The positive values for ΔH and negative slope in the van't Hoff plot for Sng-MB and Agg-MB indicate the adsorption process is endothermic for both species, and it is accompanied by an increase in the entropy of the system. Similarly, for both MB species, the process is spontaneous between 298 and 348 K, which is revealed by the negative ΔG values in this temperature range.

3.3 Adsorption Isotherm Results

Fig. 5 a) – d) show the graphs respectively for Langmuir, Freundlich, Temkin, and Dubinin-Radushkevich (D-R) isotherms. For most of the temperatures studied, the four linear isotherm models reasonably fit the results for both MB species.

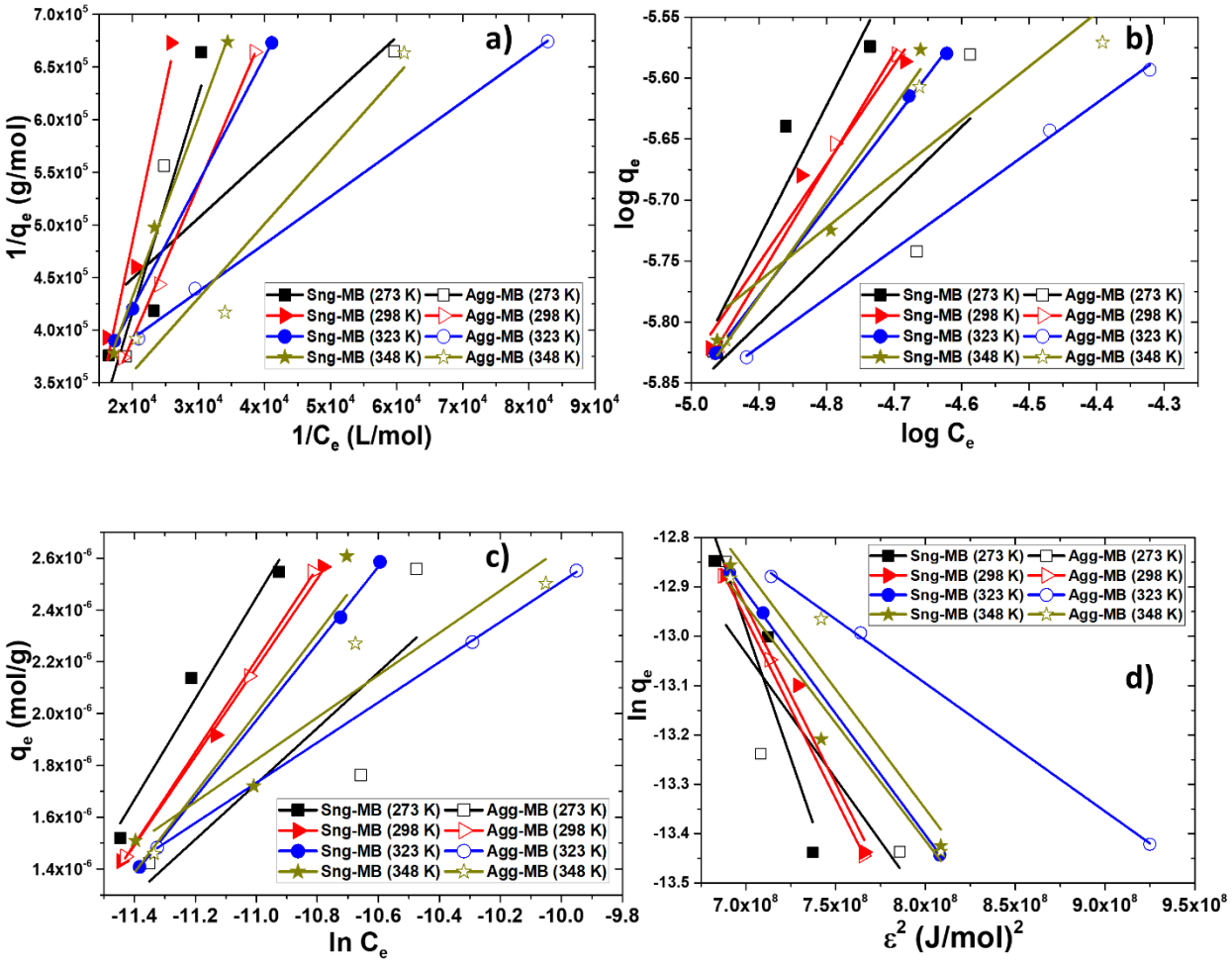

Fig. 5 Linear fitting of the adsorption isotherm models for Sng-MB and Agg-MB at different temperatures of adsorption experiment: a) Langmuir model, b) Freundlich model, c) Temkin model, and d) Dubinin-Radushkevich model.

To decide the most suitable isotherm model to describe Sng-MB and Agg-MB adsorption, the coefficient of determination (r^2) and the parameters of each isotherm model were evaluated. These results are shown in Table 3.

Table 3: Parameters obtained from linear fitting of the Langmuir, Freundlich, Temkin and Dubinin Radushkevich models for Sng-MB and Agg-MB at different temperatures:

Langmuir	Sng-MB (273 K)	Agg-MB (273 K)	Sng-MB (298 K)	Agg-MB (298 K)	Sng-MB (323 K)	Agg-MB (323 K)	Sng-MB (348 K)	Agg-MB (348 K)
K_L (L/mol)	-1.72×10^{4}	1.09×10^{5}	-8.02×10^{3}	-1.82×10^{2}	8.11×10^{3}	6.69×10^{4}	-1.35×10^{4}	1.95×10^{3}
q_m (mol/g)	-7.01×10^{-7}	1.40×10^{-6}	-1.84×10^{-6}	-4.04×10^{-4}	7.61×10^{-6}	3.32×10^{-6}	-1.26×10^{-6}	3.19×10^{-5}
r^2	0.736	0.481	0.893	0.997	0.999	0.998	0.994	0.880
Freundlich	Sng-MB (273 K)	Agg-MB (273 K)	Sng-MB (298 K)	Agg-MB (298 K)	Sng-MB (323 K)	Agg-MB (323 K)	Sng-MB (348 K)	Agg-MB (348 K)
K_F $[(mol/g)(L/g)^n]$	2.41×10^{5}	3.11×10^{-5}	2.57×10^{3}	7.13×10^{-2}	5.20×10^{-3}	1.37×10^{-4}	4.68×10^{5}	7.84×10^{-3}
1/n	2.54	0.32	2.17	1.00	0.78	0.40	2.60	0.81
r^2	0.790	0.521	0.953	0.996	0.999	0.997	0.915	0.741
Temkin	Sng-MB (273 K)	Agg-MB (273 K)	Sng-MB (298 K)	Agg-MB (298 K)	Sng-MB (323 K)	Agg-MB (323 K)	Sng-MB (348 K)	Agg-MB (348 K)
K_T	6.52×10^{8}	6.96×10^{9}	4.25×10^{8}	1.08×10^{9}	2.11×10^{9}	3.46×10^{9}	4.79×10^{8}	1.99×10^{9}
A_T (L/mol)	4.26×10^{4}	9.17×10^{5}	2.06×10^{4}	9.08×10^{4}	1.11×10^{5}	5.60×10^{5}	3.65×10^{4}	1.27×10^{5}
r^2	0.939	0.450	0.996	0.998	0.999	0.999	0.681	0.832
D-R	Sng-MB (273 K)	Agg-MB (273 K)	Sng-MB (298 K)	Agg-MB (298 K)	Sng-MB (323 K)	Agg-MB (323 K)	Sng-MB (348 K)	Agg-MB (348 K)
q_s (mol/g)	6.15×10^{-1}	5.46×10^{-6}	8.44×10^{-2}	4.05×10^{-4}	9.17×10^{-5}	1.64×10^{-5}	9.06×10^{-1}	4.21×10^{-3}
K_{DR} (mol^2/J^2)	2.42×10^{-8}	2.91×10^{-9}	1.85×10^{-8}	7.82×10^{-9}	5.27×10^{-9}	2.60×10^{-9}	1.53×10^{-8}	9.01×10^{-9}
E (kJ/mol)	-4.54	-13.1	-5.20	-8.00	-9.74	-13.9	-5.71	-7.45
r^2	0.799	0.509	0.958	0.997	0.999	0.998	0.907	0.818

For Sng-MB sample at 273 and 298 K and Agg-MB sample at 273 K, the Langmuir isotherm produced negative values for K_L and q_m, which does not comply with the physical interpretation of the result. From that, it is concluded that the Langmuir isotherm is not suitable to describe this adsorption process. The improperness of the Langmuir isotherm is expected, since it describes the adsorption of a monolayer of adsorbate on the adsorbent and is applicable for homogeneous adsorption where each molecule has the same activation energy for adsorption. This

would be unreasonable for this adsorption process, since there is the simultaneous adsorption of different MB species with different activation energy for adsorption as previously shown in section 3.1[36]. Regarding the Freundlich isotherm, the parameter 1/n is related to surface heterogeneity, and it should range between 0 and 1, with a value closer to 0 indicating higher heterogeneity of the surface[37]. The samples Sng-MB at 273, 298, and 348 K present 1/n values higher than 1, indicating the improperness of the Freundlich model to describe the adsorption process. The Temkin isotherm contains a term that accounts for the interactions between adsorbate and adsorbent, which is the Temkin isotherm equilibrium binding constant (A_T)[38]. For all temperatures, it is noticed that the Agg-MB species have higher A_T than the Sng-MB species, which can indicate a more intense interaction between Agg-MB and chitosan surface than between Sng-MB and chitosan surface. This result agrees with the kinetic result that indicated a lower activation energy for adsorption of Agg-MB in comparison to Sng-MB species, as shown in section 3.2.

Analyzing the r^2 values, D-R isotherms presented reasonably good values when compared to Temkin isotherms. For all temperatures studied, Table 3 shows that a higher isotherm saturation capacity (q_s) is obtained for Sng-MB in comparison to Agg-MB species. This can be explained by the fact that Sng-MB are smaller than Agg-MB, so for a certain chitosan surface area, it is expected to accommodate a higher number of moles of Sng-MB than Agg-MB. In contrast, the adsorption free energy (E) is higher for Agg-MB than Sng-MB for all temperatures, indicating a more intense interaction with chitosan surface for Agg-MB than Sng-MB. The adsorption free energy is generally used to infer if the interaction between adsorbate and adsorbent is chemisorption or physisorption. Generally, E with magnitude lower than 20 kJ/mol indicates the interaction proceeds through weak van der Waals forces (physisorption), whereas the energy for

chemisorption is in the range between 40 and 800 kJ/mol[39–41]. Following these criteria, it is inferred that both MB species interact with chitosan surface through weak van der Waals forces.

3.4 Structural and Optical Characterization of Chitosan samples before and after adsorption

To verify the influence of the adsorption process in the chitosan samples before and after MB species adsorption process, the XRD patterns of chitosan before and after adsorption at different temperatures were collected. As shown in Fig. 6 a), there is no difference between the XRD patterns of chitosan before and after adsorption at any of the different temperatures; this indicates the MB species adsorption process does not cause change in the crystalline structure of chitosan. The FT-IR transmittance spectra of the chitosan after adsorption for all temperatures is identical to the spectrum of the chitosan before adsorption, with the two most intense bands centered at 3415 and 1066 cm^{-1}, corresponding respectively, to superimposed stretching vibrations of OH and NH_2 and C-O stretching vibration[42]. Additionally, there is no presence of any band related to MB on the chitosan spectra after adsorption. This result may indicate there is no covalent bonding between chitosan and MB species during the adsorption process, which may also indicate that the adsorption process proceeds through physisorption, instead of chemisorption, which agrees with the results obtained in the isotherms study, as presented in section 3.3. The SEM micrographs for chitosan before and after adsorption process at 343 K presented large anisotropic grains, with the size around 70 μm. This result confirms there were no morphological changes to the chitosan during the MB species adsorption process. Chitosan samples before and after adsorption at 348 K had their surface area evaluated using N_2 BET adsorption isotherm, with both samples having

surface area around 0.40 m^2/g, indicating that chitosan surface area does not change throughout the process as well.

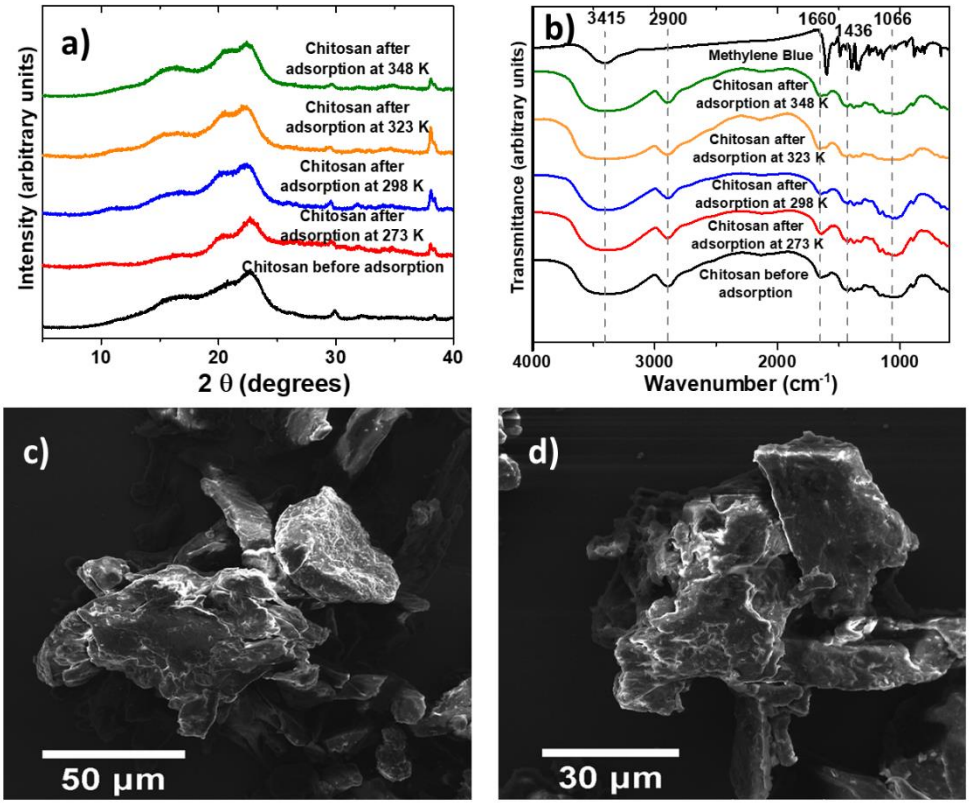

Fig.6 a) XRD patterns of chitosan before adsorption and after adsorption performed at 273, 298, 323, and 348 K, b) FT-IR transmittance spectra of chitosan before adsorption and after adsorption performed at 273, 298, 323, 348 K, and methylene blue, c) SEM image of chitosan before adsorption, and d) SEM image of chitosan after adsorption performed at 348 K.

Although neither structural nor morphological changes were observed in the chitosan before and after MB species adsorption, the optical properties changed throughout the adsorption process, as can be seen on the diffuse reflectance spectra in the visible range and photographs of the chitosan powders before and after adsorption, as it can be seen on Fig S2 and S3 in the Supporting Information. Before adsorption, chitosan did not present any reflectance peak in the visible range, whereas, after adsorption at all temperatures, it presented peaks around 566 and 656 nm, very similar to the spectrum of the methylene blue.

3.5 Insights about Metachromasy Occurrence

To elucidate the possible causes for chitosan to induce metachromasy in MB, an 8.0 x 10^{-4} mol/L (15 mg/L) MB hydrochloride solution was added to chitin at room temperature. As can be seen in Fig. S4 in Supporting Information, no peak at 560 nm was observed on MB spectrum after contact with chitin. As the only difference between the molecular structure of chitosan and chitin is the replacement of the acetyl groups from chitin by amino (NH_2) groups from chitosan, it is a reasonable hypothesis that the NH_2 groups from chitosan play a decisive role in inducing MB metachromasy. The MB metachromasy induced by NH_2 has been described in the literature; for instance, Murthy and Bhardwaj described the appearance of a new band, around 500 nm, in the MB absorption spectrum when it interacts with different types of amines, such as diethylamine, di-n-butylamine, di-isopropylamine, and n-butylamine[43]. They explained the need of NH_2 groups for a charge transfer mechanism to happen, where the cationic MB molecules act as electron acceptors, and the NH_2 groups act as electron donors[43].

To gain further mechanistic insights into the MB aggregation due to interaction with chitosan, MB aggregate sizes and their zeta potential, i.e., surface charge was determined using DLS and EPM measurement, respectively. MB solutions before adsorption onto chitosan did not produce any scattering during DLS measurements, which means no aggregates were present in the MB solution before adsorption. However, the MB solutions after adsorption onto chitosan produced a stable hydrodynamic diameter of ~450 nm, while further centrifuged MB solutions produced with ~400 nm clusters (Fig. S5). This result suggests the interactions with chitosan create stable colloidal aggregates of MB. Moreover, comparing the zeta potentials for the MB species before adsorption and MB species remaining in solution after adsorption at 348 K for 6 minutes revealed the zeta potential of the MB solution increased in magnitude from -5.5 mV before

adsorption to -39 mV after adsorption (Fig. S6). Stable colloidal aggregates typically have zeta potential more than -30 mV, thus confirming the colloidal stability of the generated MB aggregates from Agg-MB[44,45].

To test the influence of pH on the adsorption process, the initial pH of the MB solution was changed from neutral to 3 (by HCl addition) or 12 (by NaOH addition), as shown in Fig. 7, at 298 K, for a MB initial concentration of 5.3×10^{-5} mol/L. When the MB solution has an acidic pH, no peak at 560 nm is observed in the absorption spectrum, indicating acidic pH has the ability to stop the metachromasy occurrence by contact between MB and chitosan. This result confirms again that unprotonated NH_2 groups are necessary to promote MB metachromasy, since at pH values lower than 6, the NH_2 groups of chitosan become predominantly protonated (NH_3^+)[46,47].

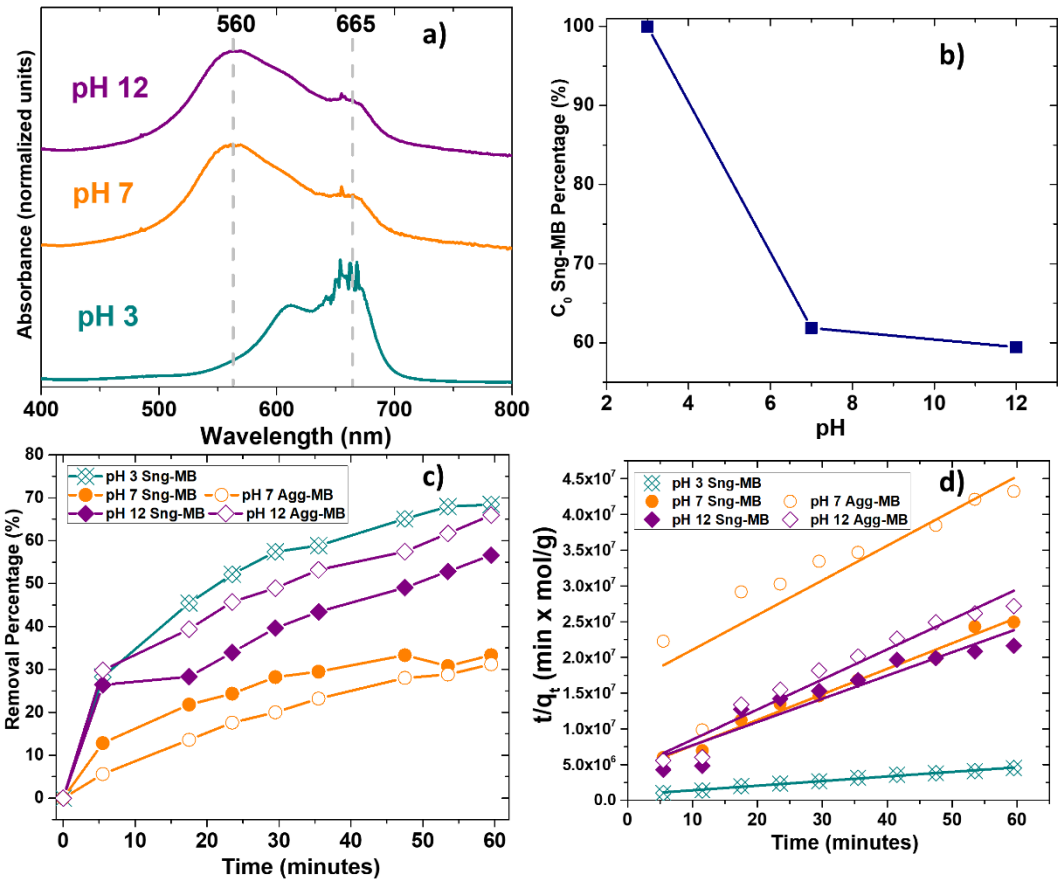

Fig. 7 a) UV-vis absorption spectra of MB samples immediately after chitosan addition, at pH values equal to 3, 7, and 12 of MB solution, at 298 K, b) Graph showing the relationship between the percentage of initial molar concentration of Sng-MB and the pH values, at 298 K, c) Removal percentage versus time of Sng-MB and Agg-MB samples at different pH values, at 298 K, d) pseudo second order adsorption kinetic models of Sng-MB and Agg-MB samples at different pH values, at 298 K.

Like the result observed for the temperature effect (Fig. 1b), an increase on pH values lead to a decrease on the initial concentration of Sng-MB produced immediately after contact between chitosan and MB, as shown in Fig. 7 b). Regarding the removal percentage, at pH 3, as only Sng-MB species is present in the solution, the highest MB removal percentage (~70%) was attained. This represents a substantial improvement in relation to the adsorption process usually carried out at pH 7, where the coexistence of Sng-MB and Agg-MB leads to a maximum removal percentage, around 30%, for each of the species. Surprisingly, when the adsorption process is carried out in

alkaline pH, a higher removal percentage for both MB species is attained. This can be explained by the fact that chitosan has a negative surface charge on pH values higher than 9, as confirmed by zeta potential measurements[48]. Consequently, the adsorption process is enhanced due to electrostatic interaction between the negatively charged chitosan and the cationic MB species.

Table 4: Adsorption capacity at equilibrium, Adsorption capacity at equilibrium per initial concentration of MB species, and rate constant estimated from the pseudo 2nd order adsorption kinetic model for Sng-MB and Agg-MB samples at different pH values.

Sample	q_e (mol/g)	q_e/C_0 (L/g)	k_2 (g.mol^{-1}.min^{-1})
Sng-MB (pH 3)	1.6×10^{-5}	5.0×10^{-2}	5.4×10^{3}
Sng-MB (pH 7)	2.6×10^{-6}	2.1×10^{-2}	5.3×10^{4}
Agg-MB (pH 7)	2.1×10^{-6}	2.8×10^{-2}	1.4×10^{4}
Sng-MB (pH 12)	3.1×10^{-6}	3.8×10^{-2}	2.4×10^{4}
Agg-MB (pH 12)	2.4×10^{-6}	4.3×10^{-2}	4.1×10^{4}

As shown in Table 4, the Sng-MB at pH 3 has the highest equilibrium adsorption capacity per initial concentration of the MB species; however, it has the lowest rate constant, which indicates that, although it has the highest removal percentage and adsorption capacity, this removal process happens at a slower rate when compared to Sng-MB and Agg-MB species at pH 7 and 12.

4. Conclusions

The temperature varying studies revealed the concentration of Sng-MB and Agg-MB initially produced after contact with chitosan is very dependent on temperature, with the concentration of Agg-MB species increasing with temperature. About the kinetics, in general, the

Agg-MB species have a higher rate constant than the Sng-MB species. The Agg-MB species also have a lower activation energy, which may indicate the adsorption of Agg-MB onto chitosan surface is preferred in relation to Sng-MB. The thermodynamic study revealed the adsorption process of either MB species is endothermic and spontaneous in most of the temperature ranges studied. The adsorption process was not found to cause any structural or morphological changes in the chitosan structure. Finally, the metachromasy process could be suppressed in acidic pH, which increased the removal efficiency of the MB, whereas in alkaline pH, although the metachromasy could not be suppressed, there was an enhancement of the removal percentage of MB species, probably due to occurrence of the electrostatic interactions between cationic MB species and the chitosan surface, which is negatively charged at alkaline pH.

Acknowledgements

The authors would like to thank Prof. Akiko Fillinger (Ithaca College, Department of Chemistry) for assistance with the scanning electron microscopy images collection, also Ithaca College Office of the Provost and Center of Faculty Excellence for financial support.

This work made use of the Cornell Center for Materials Research Facilities for SEM characterization, which is supported by the National Science Foundation under Award Number DMR-1719875.

Appendix A. Supplementary data

The following is supplementary data for this article.

(Supporting Information file)

References

[1] K.B. Tan, M. Vakili, B.A. Horri, P.E. Poh, A.Z. Abdullah, B. Salamatinia, Adsorption of dyes by nanomaterials: Recent developments and adsorption mechanisms, Sep. Purif. Technol. 150 (2015) 229–242. doi:10.1016/j.seppur.2015.07.009.

[2] Y. Wang, M. Zhu, Y. Li, M. Zhang, X. Xue, Y. Shi, B. Dai, X. Guo, F. Yu, Heteroatom-doped porous carbon from methyl orange dye wastewater for oxygen reduction, Green Energy Environ. 3 (2017) 172–178. doi:10.1016/j.gee.2017.06.005.

[3] E. Forgacs, T. Cserháti, G. Oros, Removal of synthetic dyes from wastewaters: A review, Environ. Int. 30 (2004) 953–971. doi:10.1016/j.envint.2004.02.001.

[4] T. Veuthey, Dyes and stains : From molecular structure to histological application, Front. Biosci. 19 (2014) 91–112. doi:10.2741/4197.

[5] A. Mills, D. Hazafy, J. Parkinson, T. Tuttle, M.G. Hutchings, Effect of alkali on methylene blue (C.I. Basic Blue 9) and other thiazine dyes, Dye. Pigment. 88 (2011) 149–155. doi:10.1016/j.dyepig.2010.05.015.

[6] V. Vadivelan, K. Vasanth Kumar, Equilibrium, kinetics, mechanism, and process design for the sorption of methylene blue onto rice husk, J. Colloid Interface Sci. 286 (2005) 90–100. doi:10.1016/j.jcis.2005.01.007.

[7] V. Kumar, R. Kumar, A. Nayak, A. Saleh, M.A. Barakat, Adsorptive removal of dyes from aqueous solution onto carbon nanotubes : A review, Adv. Colloid Interface Sci. 194 (2013) 24–34. doi:10.1016/j.cis.2013.03.003.

[8] R.G. Saratale, G.D. Saratale, J.S. Chang, S.P. Govindwar, Bacterial Decolorization and

Degradation of Azo Dyes : A Review Journal of the Taiwan Institute of Chemical Engineers Bacterial decolorization and degradation of azo dyes : A review, J. Taiwan Inst. Chem. Eng. 42 (2011) 138–157. doi:10.1016/j.jtice.2010.06.006.

[9] R.B. McKay, Red Forms of Methylene Blue, Nature. 210 (1966) 296–297. doi:10.1038/210296a0.

[10] H. Terayama, On the nature of metachromasy, Jpn. Med. J. (Natl. Inst. Health. Jpn). 2 (1949) 137–149. doi:10.7883/yoken1948.2.137.

[11] R. Dobritoiu, S. Patachia, A study of dyes sorption on biobased cryogels, Appl. Surf. Sci. 285 (2013) 56–64. doi:10.1016/j.apsusc.2013.07.164.

[12] D. Ziółkowska, A. Kaniewska, J. Lamkiewicz, A. Shyichuk, Determination of carrageenan by means of photometric titration with Methylene Blue and Toluidine Blue dyes, Carbohydr. Polym. 165 (2017) 1–6. doi:10.1016/j.carbpol.2017.02.029.

[13] B. Heyne, Self-assembly of organic dyes in supramolecular aggregates, Photochem. Photobiol. Sci. 15 (2016) 1103–1114. doi:10.1039/C6PP00221H.

[14] A.X.P. D'mello, T.V. Sylvester, V. Ramya, F.P. Britto, P.K. Shetty, S. Jasphin, Metachromasia and Metachromatic Dyes : A review, Int. J. Adv. Heal. Sci. 2 (2016) 12–17.

[15] K. Yurekli, E. Conley, R. Krishnamoorti, Effect of Laponite and a Nonionic Polymer on the Absorption Character of Cationic Dye Solutions, Langmuir. 21 (2005) 5825–5830. doi:10.1021/la047540k.

[16] J. Cenens, R.A. Schoonheydt, Visible Spectroscopy of Methylene Blue on Hectorite,

Laponite B, and Barasym in Aqueous Suspension., Clays Clay Miner. 36 (1988) 214–224. doi:10.1346/CCMN.1988.0360302.

[17] K. Haubner, J. Murawski, P. Olk, L.M. Eng, C. Ziegler, B. Adolphi, E. Jaehne, The route to functional graphene oxide, ChemPhysChem. 11 (2010) 2131–2139. doi:10.1002/cphc.201000132.

[18] D.B. Tada, L.L.R. Vono, E.L. Duarte, R. Itri, P.K. Kiyohara, M.S. Baptista, L.M. Rossi, Methylene blue-containing silica-coated magnetic particles: A potential magnetic carrier for photodynamic therapy, Langmuir. 23 (2007) 8194–8199. doi:10.1021/la700883y.

[19] V.K. Gupta, Suhas, Application of low-cost adsorbents for dye removal - A review, J. Environ. Manage. 90 (2009) 2313–2342. doi:10.1016/j.jenvman.2008.11.017.

[20] L. Zhang, Y. Zeng, Z. Cheng, Removal of heavy metal ions using chitosan and modi fi ed chitosan : A review, J. Mol. Liq. 214 (2016) 175–191. doi:10.1016/j.molliq.2015.12.013.

[21] P. Kumar Dutta, J. Dutta, V.S. Tripathi, Chitin and chitosan: Chemistry, properties and applications, J. Sci. Ind. Res. 63 (2004) 20–31. doi:10.1002/chin.200727270.

[22] I. Aranaz, M. Mengíbar, R. Harris, I. Paños, B. Miralles, N. Acosta, G. Galed, Á. Heras, Functional Characterization of Chitin and Chitosan, (2009) 203–230.

[23] L. Csoka, T.R. Appel, A. Eitner, G. Jirikowski, J. Makovitzky, Polarization optical-histochemical characterization and supramolecular structure of carbohydrate fibrils, Acta Histochem. 115 (2013) 22–31. doi:10.1016/j.acthis.2012.03.003.

[24] S. Hirano, J. Kinugawa, A. Nishioka, H. Tino, Transformation of triplet induced Cotton effects of the methylene blue complexes of some sulphate derivatives of chitosan, Int. J.

Biol. Macromol. 9 (1987) 11–14. doi:10.1016/0141-8130(87)90018-3.

[25] E. Rabinowitch, L.F. Epstein, Polymerization of Dyestuffs in Solution. Thionine and Methylene Blue, J. Am. Chem. Soc. 63 (1941) 69–78. doi:10.1021/ja01846a011.

[26] S. Sen Gupta, K.G. Bhattacharyya, Kinetics of adsorption of metal ions on inorganic materials: A review, Adv. Colloid Interface Sci. 162 (2011) 39–58. doi:10.1016/j.cis.2010.12.004.

[27] Y.S. Ho, G. Mckay, A Comparison of Chemisorption Kinetic Models Applied To Pollutant Removal on Various Sorbents, Process Saf. Environ. Prot. 76 (1998) 332–340. doi:10.1205/095758298529696.

[28] H. Qiu, L. Lv, B. Pan, Q. Zhang, W. Zhang, Q. Zhang, Critical review in adsorption kinetic models, J. Zhejiang Univ. Sci. A. 10 (2009) 716–724. doi:10.1631/jzus.A0820524.

[29] M. Doğan, M. Alkan, A. Türkyilmaz, Y. Özdemir, Kinetics and mechanism of removal of methylene blue by adsorption onto perlite, J. Hazard. Mater. 109 (2004) 141–148. doi:10.1016/j.jhazmat.2004.03.003.

[30] A. Bera, T. Kumar, K. Ojha, A. Mandal, Adsorption of surfactants on sand surface in enhanced oil recovery: Isotherms, kinetics and thermodynamic studies, Appl. Surf. Sci. 284 (2013) 87–99. doi:10.1016/j.apsusc.2013.07.029.

[31] N.A. Travlou, G.Z. Kyzas, N.K. Lazaridis, E.A. Deliyanni, Graphite oxide/chitosan composite for reactive dye removal, Chem. Eng. J. 217 (2013) 256–265. doi:10.1016/j.cej.2012.12.008.

[32] Ã. Crini, P. Badot, Application of chitosan , a natural aminopolysaccharide , for dye

removal from aqueous solutions by adsorption processes using batch studies : A review of recent literature, 33 (2008) 399–447. doi:10.1016/j.progpolymsci.2007.11.001.

[33] K.Y. Foo, B.H. Hameed, Insights into the modeling of adsorption isotherm systems, Chem. Eng. J. 156 (2010) 2–10. doi:10.1016/j.cej.2009.09.13.

[34] D.K. Singh, V. Kumar, V.K. Singh, S.H. Hasan, Modeling of adsorption behavior of the amine-rich GOPEI aerogel for the removal of As (III) and As (V) from aqueous media, RSC Adv. 6 (2016) 56684–56697. doi:10.1039/c6ra10518a.

[35] I. Moreno-Villoslada, C. Torres-Gallegos, R. Araya-Hermosilla, H. Nishide, Influence of the linear aromatic density on methylene blue aggregation around polyanions containing sulfonate groups, J. Phys. Chem. B. 114 (2010) 4151–4158. doi:10.1021/jp909105r.

[36] S.J. Allen, G. Mckay, J.F. Porter, Adsorption isotherm models for basic dye adsorption by peat in single and binary component systems, J. Colloid Interface Sci. 280 (2004) 322–333. doi:10.1016/j.jcis.2004.08.078.

[37] F. Haghseresht, G.Q. Lu, Adsorption Characteristics of Phenolic Compounds onto Coal-Reject-Derived Adsorbents, Energy and Fuels. 12 (1998) 1100–1107. doi:10.1021/ef9801165.

[38] Y. Kim, C. Kim, I. Choi, S. Rengaraj, J. Yi, Arsenic Removal Using Mesoporous Alumina Prepared via a Templating Method, Environ. Sci. Technol. 38 (2004) 924–931. doi:10.1021/es0346431.

[39] J. Kluczka, M. Gnus, A. Kazek-Kęsik, G. Dudek, Zirconium-chitosan hydrogel beads for removal of boron from aqueous solutions, Polymer (Guildf). 150 (2018) 109–118.

doi:10.1016/j.polymer.2018.07.010.

[40] M.M. Walczak, P.K. Leavitt, P.A. Thiel, Oxygenated Fluorocarbons Adsorbed at Metal Surfaces: Chemisorption Bond Strengths and Decomposition, J. Am. Chem. Soc. 109 (1987) 5621–5627. doi:10.1021/ja00253a010.

[41] H. Teng, E.M. Suuberg, Chemisorption of nitric oxide on char. 1. Reversible nitric oxide sorption, J. Phys. Chem. 97 (1993) 478–483. doi:10.1021/j100104a033.

[42] Q. Du, J. Sun, Y. Li, X. Yang, X. Wang, Z. Wang, L. Xia, Highly enhanced adsorption of congo red onto graphene oxide/chitosan fibers by wet-chemical etching off silica nanoparticles, Chem. Eng. J. 245 (2014) 99–106. doi:10.1016/j.cej.2014.02.006.

[43] A.S.N. Murthy, A.P. Bhardwaj, Electronic absorption spectroscopic studies on the red form of methylene blue ion, Proc. Indian. Acad. Sci. (Chem. Sci.). 89 (1980) 463–468. doi:10.1007/BF02881061.

[44] N. Aich, J.R. V Flora, N.B. Saleh, Preparation and characterization of stable aqueous higher-order fullerenes, Nanotechnology. 23 (2012) 055705. doi:10.1088/0957-4484/23/5/055705.

[45] N. Aich, L.K. Boateng, I.V. Sabaraya, D. Das, J.R.V. Flora, N.B. Saleh, Aggregation Kinetics of Higher-Order Fullerene Clusters in Aquatic Systems, Environ. Sci. Technol. 50 (2016) 3562–3571. doi:10.1021/acs.est.5b05447.

[46] R. Navarro, J. Guzmán, I. Saucedo, J. Revilla, E. Guibal, Recovery of Metal Ions by Chitosan: Sorption Mechanisms and Influence of Metal Speciation, Macromol. Biosci. 3 (2003) 552–561. doi:10.1002/mabi.200300013.

[47] Q.Z. Wang, X.G. Chen, N. Liu, S.X. Wang, C.S. Liu, X.H. Meng, C.G. Liu, Protonation constants of chitosan with different molecular weight and degree of deacetylation, Carbohydr. Polym. 65 (2006) 194–201. doi:10.1016/j.carbpol.2006.01.001.

[48] G. Bajaj, W.G. Van Alstine, Y. Yeo, Zwitterionic chitosan derivative, a new biocompatible pharmaceutical excipient, prevents endotoxin-mediated cytokine release, PLoS One. 7 (2012). doi:10.1371/journal.pone.0030899.